Experimental and theoretical x-ray magnetic-circular-dichroism study of the magnetic properties of $Co_{50}Pt_{50}$ thin films

W. Grange, I. Galanakis, M. Alouani, and M. Maret
Institut de Physique et Chimie des Matériaux de Strasbourg (IPCMS), 23 rue du Loess, 67037 Strasbourg Cedex, France

J.-P. Kappler*
Laboratoire pour l'Utilisation du Rayonnement Electromagnétique (LURE), BP 34, 91898 Orsay Cedex, France

A. Rogalev
European Synchrotron Radiation Facility (ESRF), BP 220, 38043 Grenoble Cedex, France
(Received 13 January 1999; revised manuscript received 21 January 2000)

An experimental and theoretical investigation of the structural and micromagnetic properties of the $Co_{50}Pt_{50}$ ordered alloy is presented. The Co-3*d* and Pt-5*d* orbital and spin magnetic moments and their anisotropies are determined by means of angle-dependent x-ray magnetic-circular-dichroism (XMCD) measurements. Our calculated spin magnetic moments of both Co and Pt are in good agreement with our experimental results, while the orbital magnetic moments are underestimated. The reduction of the 3*d* and 5*d* orbital magnetic moments, observed when the spin magnetic moment is forced out of the easy axis of magnetization, is reproduced by the theory. The calculated XMCD reproduces semiquantitatively the experimental spectra and underestimates the so-called branching ratio. The computed magnetocrystalline anisotropy is of the same order of magnitude as the experimental one with the correct sign.

I. INTRODUCTION

Molecular-beam epitaxy (MBE) has several capabilities not afforded by conventional bulk techniques, that can contribute in the fabrication of artificial materials with peculiar properties. In particular, it has been demonstrated that a tunable magnetocrystalline anisotropy (MCA) could be achieved in metastable (111) $CoPt_3$ thin-film alloys, simply by changing the growth temperature.[1,2] The appearance of this growth-induced chemical anisotropy in thin films grown around 690 K was closely connected to the formation of anisotropic local order effects [i.e., the formation of small Co in-plane two-dimensional (2D) clusters embedded in Pt] induced by a preferential surface diffusion together with a Pt segregation at the growth surface.[3] The large perpendicular magnetocrystalline anisotropy (PMA) found in this system (10^7 erg cm^{-3}) and its relative small Curie temperature (close to 500 K) make $CoPt_3$ thin films good candidates for magneto-optic recording applications.[4] One should note, however, that a small increase in the growth temperature favors the formation of the equilibrium phase, which is of the $L1_2$-type. Consequently, a variation in the MCA by a factor of about 5 is found for an increase in the growth temperature of only 60 K.

As mentioned above, the mechanisms that govern MCA in CoPt alloy systems are often local order effects and it is therefore difficult for the theory to reproduce the trends observed in experiments. The situation is, however, much more simple for $Co_{50}Pt_{50}$ alloys since a large PMA (up to 4×10^7 erg cm^{-3})[5] is observed for the ordered tetragonal $L1_0$-type equilibrium phase (i.e, alternating layers of pure Co and Pt atoms, see Fig. 1). For bulk systems, single ordered crystals are obtained from the disordered state by annealing up to 1000 K in the presence of a magnetic field. For thin films grown by MBE, a preferential ordering direction can be directly achieved *via* the effects mentioned above and by an appropriate choice of substrates. In contrast to what is observed for $CoPt_3$ thin films, an increase in the growth temperature (or, in other words, in the bulk mobility) up to the order-disordered transition should favor the formation of the $L1_0$-type crystal structure and consequently PMA. Therefore, a large and constant MCA can be easily obtained from a wide range of growth temperature.

MCA can be probed by many techniques such as torque or ferromagnetic resonance measurements. Both these methods are not element specific, they cannot distinguish between the shape and the magnetocrystalline anisotropies and characterize MCA in terms of phenomenological anisotropy constants. It has been recently demonstrated by Weller *et al.*[6] that x-ray magnetic circular dichroism (XMCD) is also a suitable technique to probe MCA, *via* the determination of the anisotropy of the orbital magnetic moment on a specific shell and site. This new technique gives therefore a clear picture of the mechanisms involved in the appearance of MCA in thin films.[7]

Several *ab initio* calculations have already been performed to investigate the XMCD.[8,9] The L_2 and L_3 edges involving electronic excitations of 2*p*-core electrons towards *d*-valence states have primarily attracted much attention due to the dependence of the dichroic spectra on the exchange-splitting and the spin-orbit coupling of both initial core and final valence states. For 5*d* elements dissolved in 3*d* transition metals, the spin-orbit coupling of the initial 2*p*-core states is large and the resulting magnetic moment is small, while the opposite is true for the 3*d* elements. This can lead to pronounced dichroic spectra as seen by Schütz in the case

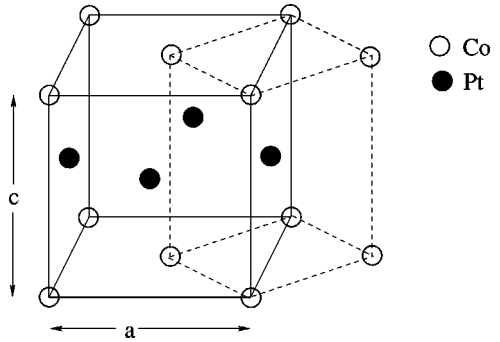

FIG. 1. Schematic representation of the $L1_0$-type crystal structure and corresponding tetragonal unit cell used in the electronic structure calculations. Note that the $Co_{50}Pt_{50}$ ordered alloy can be viewed as a film of alternating Co and Pt layers.

of 5*d* elements dissolved in Fe.[10] Calculations performed by Ebert for a disordered $Co_{80}Pt_{20}$ system,[8] have shown that the spin-orbit coupling of the final states is rather unimportant for the XMCD on the Co atom while the exchange splitting of the 2*p*-core states made a remarkable contribution. But obviously, the major contributions came from the spin-orbit coupling of the core states and the exchange-splitting of the conduction states. For the Pt atom, the spin-orbit coupling of the core states and the exchange splitting of the conduction states play the same role as well as the final states spin-orbit coupling.

Brouder *et al.*,[11,12] Guo,[13] and Ankudinov *et al.*[14,15] used multiple scattering theory to study XMCD but their method is time consuming for systems with a large number of atoms. Finally, atomic calculations in crystal-field symmetry are widely applied to describe the $M_{4,5}$ edges of rare earths and actinides and the $L_{2,3}$ edges of transition metals. Because of the large number of parameters to fit, it is difficult to apply this formalism to delocalized 3*d* states.[16]

In this paper, we present an experimental analysis on the growth, the macroscopic magnetic properties and the micromagnetism of a $Co_{50}Pt_{50}$ thin film grown on a MgO (001) substrate at 800 K. A special emphasis is given on the determination of the Co-3*d* and Pt-5*d* orbital and spin magnetic moments from XMCD measurements. In particular, angle-dependent XMCD measurements outline the mechanisms that are responsible for a large MCA in CoPt systems. Finally, an *ab initio* investigation of the magnetic properties (magnetic moments, MCA, XMCD) by means of a fully relativistic and spin-polarized full-potential linear muffin-tin orbital method (FP-LMTO) is presented. The experimental trends are well reproduced by our theory.

II. EXPERIMENTAL

A. Sample preparation and structural analysis

The 40-nm $Co_{50}Pt_{50}$ thin film was co-deposited at 800 K under UHV conditions on a (001) MgO substrate, following the growth of a 9-nm Pt buffer layer grown at 990 K. Great care was taken to clean the substrate and different *in situ* annealing treatments ensured the desorption of H_2O and CO molecules from the surface.[17] The rate of deposition was 0.011 and 0.008 $nm.s^{-1}$ for the Pt and Co atoms, respectively. The sample was finally capped with a 3-nm Ru layer

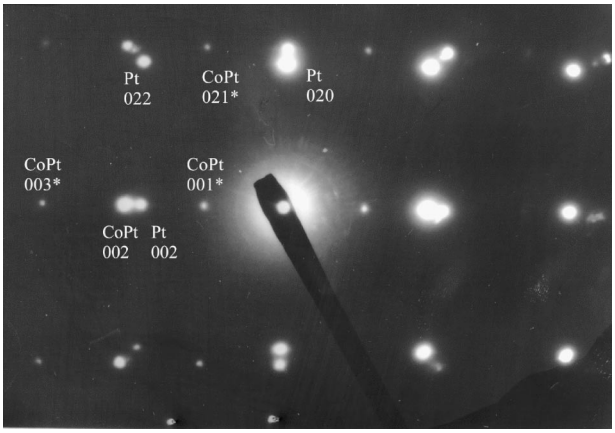

FIG. 2. The microdiffraction patterns obtained by transmission electron microscopy in the $Co_{50}Pt_{50}$ thin film. For this experiment, the incident electron beam is along the MgO [100] direction. The asterisks indicate the reflections that are normally absent for a disordered alloy.

to prevent oxidation. The structural analysis was performed *ex situ* by transmission electron microscopy (TEM) and x-ray diffraction (XRD) measurements. The TEM measurements were performed on a high-resolution transmission electron microscope (TOPCON, 200 keV) and the XRD measurements were performed on a high-resolution x-ray diffractometer using Cu $K\alpha$ radiation. TEM measurements were performed in cross-section and plane view samples, i.e., the incident electron beam is along the MgO [100] azimuth and the MgO [001] growth direction, respectively. The electron-diffraction pattern of the cross-section sample shows the 002 Pt and 002 CoPt diffraction spots (Fig. 2), and more interestingly intermediate spots such as the labeled 001 spot at half the distance between the transmitted beam and the 002 CoPt spot, and also the 021 spot between the 020 and 022 ones. Such reflections, extinguished in a fcc disordered CoPt alloy, are the signature of a chemical ordering along the growth direction. The corresponding TEM diffraction pattern of the plane view sample (not shown), evidence (in addition of the 200 and 020 CoPt fundamental spots) supplementary spots, labeled 110, characteristic of a $L1_0$-type ordering. The absence of both the 100 and 010 spots reveals that only $L1_0$-type ordered regions with the *c* axis along the growth direction are present. We recall that the first observation of the $L1_0$ long-range order (LRO) for a (001) CoPt thin film grown by MBE was made by Harp *et al.* in 1993.[18] More recently, the growth of a $L1_0$ phase was also achieved in a MBE co-deposited FePd film.[19]

The MBE process is therefore clearly inequivalent to conventional bulk methods for which ordering may occur along any principal crystallographic direction. This should be related to two different effects that are discussed in details in the following: (i) the influence of the buffer layer (ii) the Pt segregation at the growth surface. For a growth temperature of 800 K [close to the order-disorder transition (1100 K)], we expect naturally the formation of the tetragonal $L1_0$ phase. The influence of the Pt buffer layer should be regarded as an external constraint for the growth [similarly to the presence of a magnetic field during annealing for conventional bulk technique (Ref. 5)]: the lattice parameter of Pt fcc is 0.392 nm [that is much larger than the *c* parameter of the $L1_0$

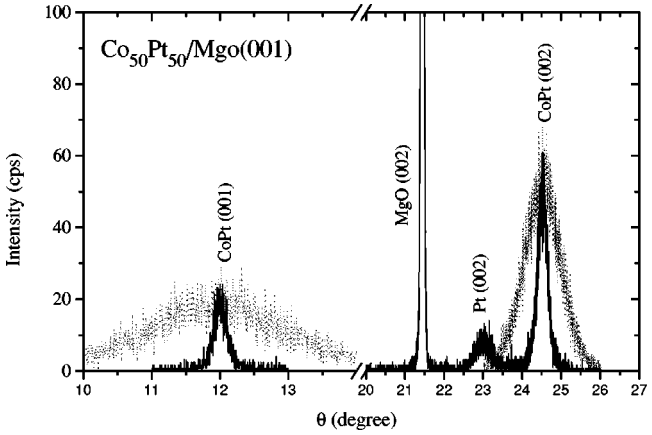

FIG. 3. Solid line: specular x-ray diffraction of the $Co_{50}Pt_{50}$ thin film grown at 800 K on MgO (001). Dashed curve: corresponding rocking curves. The 001 CoPt reflection is the signature of the $L1_0$ long-range order (LRO). Note that the LRO parameter can be deduced from the ratio of the (001) and (002) x-ray integrated intensities.

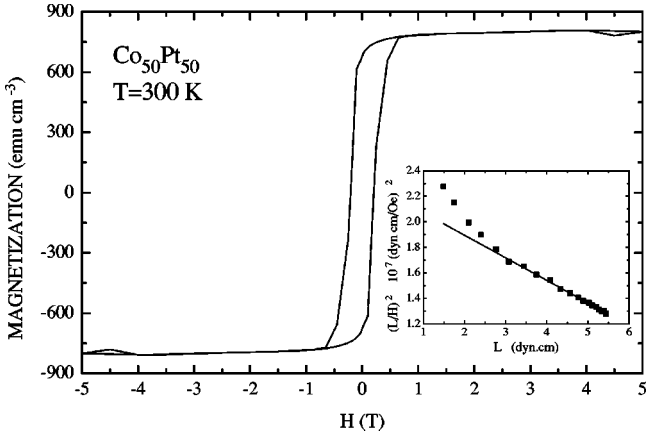

FIG. 4. The SQUID hysteresis loop measured with the applied magnetic field parallel to the surface normal. Inset: the square of the ratio of the magnetic torque L to the applied magnetic H as a function of the magnetic torque (dots). For this experiment, the magnetic field was applied at 45° away from the normal to the surface. The solid line is a fit assuming that $(L/H)^2$ varies as $-(M^2V/2K)L+(MV)^2/2$, where M denotes the total magnetization, V is the magnetic volume and $K=K_1+K_2-2\pi M^2$ (see Sec. II B).

phase (0.369 nm), but close to the a parameter of the $L1_0$ phase (0.381 nm)]. There is, therefore, a tendency for the tetragonalization along the [001] growth direction. The occurrence of a layer by layer growth can be also greatly enhanced by a dominant surface diffusion associated with a Pt segregation along the advancing surface during growth. This latter effect can lead to the formation of an alternation of Pt-rich and Pt-poor planar regions perpendicular to the growth direction, similarly to what happens for (111) $CoPt_3$ thin films grown at 690 K.[2,20] Finally, these two combined effects yield the formation of an almost perfect superlattice constituted of alternating Co and Pt layers perpendicular to the growth direction.

The importance of chemical LRO in the CoPt film can be characterized by an order parameter defined as the difference between the Co atomic concentrations in the Co-rich and Co-poor (001) planes. The determination of this parameter from the ratio of the 001 and 002 electron spot intensities is really inaccurate and it is more judicious to use the x-ray integrated intensities of the fundamental and superlattice reflections. Figure 3 shows the $\theta-2\theta$ scans around the 001 superlattice and 002 fundamental peaks (solid curve); the dashed curves are the rocking curves around these reflections. The normal coherence length deduced from the full width at half maximum (FWHM) of the 002 peak (solid curve) is about 15 nm, and the mosaic spread given by the FWHM of the corresponding rocking curve is equal to 1.1°. The chemical LRO parameter deduced from the ratio of the x-ray integrated intensities of the superlattice and fundamental reflections, corrected for absorption and Lorentz-polarization factors, is close to 0.6 ± 0.1. This value represents an average and apparent LRO through the total thickness of the film. A more precise description of LRO from the analysis of high resolution TEM images will be published elsewhere.

B. Magnetic measurements

In this section, we first briefly discuss the results obtained from macroscopic measurements that allow us to determine the total magnetization and the anisotropy energy. The Co-$3d$ and Pt-$5d$ orbital and spin magnetic moments and their anisotropies will be determined using angle-dependent XMCD measurements.

Magnetization measurements were performed using superconducting quantum interference device (SQUID) at 300 K with the field applied parallel or perpendicular to the film plane (Fig. 4). The total magnetization was found to be (780 ± 50) emu cm^{-3}. In the parallel geometry, the saturation of the magnetization was not achieved for the range of field available (up to 7 T), which illustrates the large magnetocrystalline anisotropy. We note, however, that the sample is fully saturated if the magnetic field is applied at 45° or even 60° with respect to the normal to the surface ($H_{sat}=1$ T and 4 T, respectively).

To determine the anisotropy energy, we have performed torque measurements using the 45° method proposed by Miyajima and Sato.[21] This method ensures a quantitative determination of the quantity $K=K_1+K_2$ (the sum of the second and fourth anisotropy constants) by measuring the magnetic torque as a function of the magnitude of the applied magnetic field at a fixed angle, i.e., at 45° away from a direction of easy or hard magnetization axis. From this measurement (shown in the inset of Fig. 4), we have deduced a K value of $(3.0\pm0.5)\times10^7$ erg cm^{-3}. This value is slightly smaller than the one reported by Eurin and Pauleve from their magnetic measurements performed on a bulk single crystal ($K=4\times10^7$ erg cm^{-3}).[5] We attribute this difference to the smallest chemical ordering found in our sample.

1. Probing MCA with XMCD

We now present the results of high-field angle-dependent XMCD measurements at both the Co and Pt $L_{2,3}$ edges in the $Co_{50}Pt_{50}$ thin film. In the following sections, these results (namely, the determination of the local magnetic moments on both the Co and Pt atoms and their variation as a function

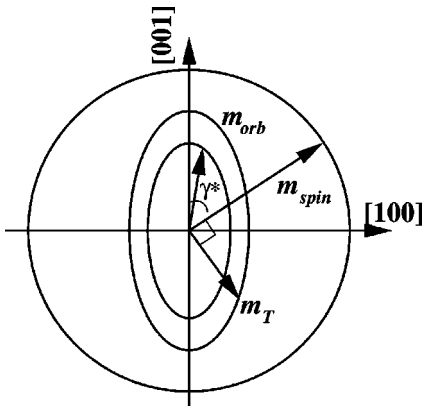

FIG. 5. The angle dependence of the ground-state magnetic moments for a $3d$ transition metal and an uniaxial symmetry (i.e., in second-order perturbation theory). γ denotes the angle between the direction of the spin magnetic moment (the direction of the applied magnetic field) and the normal to the surface, i.e., the [001] direction. m_{spin} describes a circle whereas $m_{orb}\,(m_T)$ describes an ellipse when the magnetic field (large enough to magnetically saturate the sample) is rotated in the (010) plane (Ref. 31). For a ''magic angle,'' $\gamma^{\star}=57.3°$, m_T and m_{spin} are perpendicular and the effective spin moment calculated by the sum rules is equal to the spin moment.

of the angle between the x-ray beam and the normal to the surface) will be compared with the results of our *ab initio* calculations. For convenience, the derived $3d\,(5d)$ orbital and spin magnetic moments will be expressed per number of $3d\,(5d)$ holes.

The XMCD is defined as the difference in absorption for right- and left-handed circularly polarized light, when the magnetic field is parallel to the x-ray wave vector. We have used the optical sum rules to get a reliable information on the micromagnetism (i.e., the separation and the determination of the spin and orbital magnetic moments on a specific shell and site), directly from the experimental spectra.[22,23] Still currently, the application of the XMCD sum rules—in particular for low symmetry systems—is debated since the quantity determined from the second sum rule is an effective spin magnetic moment m_{spin}^{eff} (the spin magnetic moment m_{spin} and the magnetic dipole term m_T, see Fig. 5).[23–25] The determination of the orbital magnetic moment m_{orb} is less difficult and can be of great importance for the determination of MCA.

In some particular cases, Bruno showed that the MCA could be related to the anisotropy of the orbital magnetic moment $E^{MCA}\sim\xi(m_{orb}^{z}-m_{orb}^{x})$, where ξ denotes the spin-orbit coupling constant and $(m_{orb}^{z}-m_{orb}^{x})$ is the angular variation of the orbital magnetic moment (z and x denote two principal cryotallographic directions).[27–29] The angle-dependent XMCD measurements have therefore gained considerable attention from experimentalists since they allow, in principle, a quantitative determination of the orbital moment. The advantage of Bruno's relation is the qualitative explanation of the enhancement of the MCA in thin films; at the surface, the breaking of symmetry leads to a strong difference in the band width for the in-plane and out-of-plane orbitals.[30] This yields strongly anisotropic orbital magnetic moments and therefore a large MCA. Despite the corrections by van der Laan[31] of Bruno's relation, when holes are also present in the spin-up band, it remains difficult to obtain a quantitative value of the MCA energy from XMCD. For this reason, the magnetic anisotropy energy will be discussed only qualitatively in terms of the orbital magnetic moment. We should, however, state that the main advantage of XMCD over conventional techniques such as torque measurements is that XMCD is element specific. Therefore, the role of the Pt atoms in the appearance of MCA will be also discussed.

2. XMCD at the Co $L_{2,3}$ edges

XMCD experiments were performed at the European Synchrotron Radiation Facilities (ESRF) on the ID12B (Co $L_{2,3}$ edges) beamline.[32] We have used a collinear geometry for which the applied magnetic field is parallel to the incident photon beam. The x-ray absorption (XAS) spectra were monitored at room temperature in the total electron yield detection mode. For all these experiments, we have found that a 5-T applied magnetic field was large enough to saturate the sample. The XMCD signal was obtained by reversing the direction of the magnetic field, keeping the helicity of the incoming photons fixed. The circular polarization rate was estimated to be 0.85.[33]

In the collinear geometry, the angle-dependent orbital sum rule for XMCD takes the following form [we define γ as the angle between the normal to the surface (z axis, [001] direction) and the direction of the applied magnetic field]:

$$m_{orb}^{\gamma}=-(2Q^{\gamma}/3R)h_{3d}, \tag{1}$$

where m_{orb}^{γ} denotes the $3d$ orbital magnetic moment measured at the angle γ, Q^{γ} is the integrated dichroism intensity over the L_3 and L_2 edges at the angle γ (corrected for the incomplete polarization of the x rays), R is the integrated $3d$ isotropic absorption cross section (which is angle independent), and h_{3d} is the corresponding isotropic number of holes in the $3d$ shell (see Fig. 6).

As shown in Fig. 7, the integrated XMCD signal is anisotropic, and hence via Eq. (1) so is the $3d$ orbital magnetic moment (it is reduced by a factor of about 2 for $\gamma=60°$ as can been seen in Table I). Assuming uniaxial symmetry, the orbital magnetic moment in the film plane can be evaluated from the following variation:[31,34] $m_{orb}^{\gamma}=m_{orb}^{z}+(m_{orb}^{x}-m_{orb}^{z})\sin^2\gamma$, where x refers to the [100] direction. We found $m_{orb}^{z}/h_{3d}=0.10\mu_B$ and $(m_{orb}^{z}-m_{orb}^{x})/h_{3d}=0.08\mu_B$ (per Co atom), resulting in an anisotropy of the $3d$ orbital magnetic moment of 170% of its isotropic value $[(m_{orb}^{z}+2m_{orb}^{x})/3]$. By comparison, the value found in a $CoPt_3$ thin film grown at 690 K was only about 60%.[34] Note here that Bruno's relation states that the easy axis of magnetization lies along the maximum orbital moment direction for hard ferromagnets. We therefore expect XMCD measurements to confirm the presence of PMA. Finally, typical errors in the determination of the orbital magnetic moment are of the order of 10%, while error bars for spin moments vary from 6% to 10% slightly larger compared to previous experiments that estimated the experimental error bar to be 4% for both orbital and spin moments.[24]

From the spin sum rule, we derive an effective spin magnetic moment per $3d$ hole of 0.75 $\mu_B\,(\gamma=0°)$. Although the contribution of the magnetic dipole term is expected to be small in $3d$ metals, it cannot be ignored in our case since the

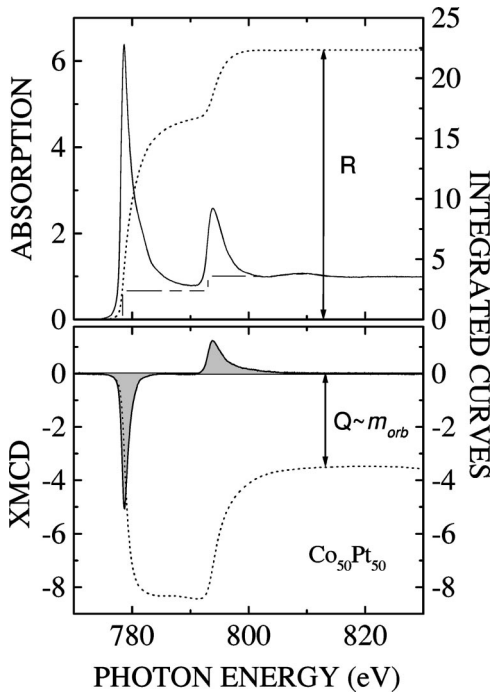

FIG. 6. Top panel. Solid line: the isotropic absorption cross section (the half-sum of the absorption spectra recorded for a parallel and antiparallel alignment of the photon spin and the magnetization vector) measured at the $L_{2,3}$ edges of Co in the $Co_{50}Pt_{50}$ thin film ($\gamma=0°$). Squares: a step-height function that accounts for the transitions towards the continuum states. The $3d$ absorption cross section is the difference between these two latter curves. Lower panel: the corresponding XMCD signal (the difference in the absorption spectra recorded for an antiparallel and parallel alignment of the photon spin and the magnetization vector). The R and Q integrals (dots) are the quantities appearing in the orbital sum rule (see text). The XMCD signal is corrected for the circular polarization rate (0.85). Note that the Q integral is directly proportional to the orbital magnetic moment of the $3d$ shell.

$L1_0$-type structure is highly anisotropic. The separation of the magnetic moment can be *a priori* obtained from the angle dependence of the effective spin magnetic moment itself.[6,35] Since, for a $3d$ transition metal, the magnetic dipole term only describes a quadripolar term in the spin charge distribution around the nucleus, it can be written as $m_T = Q^{\star}\hat{\mathbf{S}}$, where $\hat{\mathbf{S}}$ is a unit vector along the direction of the spin magnetic moment and $Q^{\star}$ is a second-rank tensor with vanishing trace. There should therefore exist an angle (known as the ''magic angle'') for which the projection of m_T along m_{spin} vanishes (Fig. 5). For this angle ($\gamma^{\star} = 57.3°$), we obtain $m_{spin}/h_{3d} = 0.67\,\mu_B$ (per Co atom).

3. XMCD at the Pt $L_{2,3}$ edges

In a previous paper,[34] we have outlined the role played by the $5d$ electrons in the appearance of MCA. The enhancement of MCA found in CoPt systems could result from: (i) the enhancement in the anisotropy of the Co-$3d$ magnetic moment due to an anisotropic $3d$-$5d$ hybridization, (ii) the Pt-$5d$ orbital magnetic moment itself and the associated strong $5d$ spin-orbit coupling. For instance, an anisotropic $3d-5d$ hybridization causes a large difference in the in-plane V_x, and out-of-plane V_z, bandwidth of the Co $3d$ orbitals. In the $Co_{50}Pt_{50}$ ordered alloy we have $V_z > V_x$ ($m_z^{\rm orb} > m_x^{\rm orb}$) and consequently a large PMA.[7,36] The XMCD experiments at the Pt $L_{2,3}$ edges were performed at ESRF on the ID12A beamline[32] in the total fluorescence detection mode, using a collinear geometry. The experimental setup for these experiments was the same as for the one used for the experiments performed at the Co $L_{2,3}$ edges. Note that the penetration depth of the incoming x rays is about a few microns at the $L_{2,3}$ edges of Pt for a 50 nm CoPt thin films. Therefore, these experiments appeared as rather challenging.

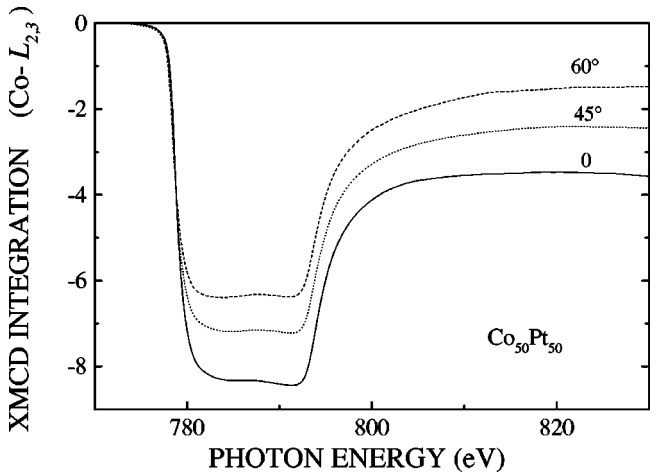

FIG. 7. The angle dependence of the integrated XMCD intensity (corrected for the incomplete polarization of the x rays) at the Co $L_{2,3}$ edges in the $Co_{50}Pt_{50}$ thin film ($\gamma=0°$, solid line; $\gamma=45°$, dots; $\gamma=60°$, dashed line).

Figure 8 shows the XMCD signal recorded at the $L_{2,3}$ of Pt in the $Co_{50}Pt_{50}$ thin film for different values of the incident angle γ. An angle dependence in the Pt-XMCD signal (or, in other words, in the $5d$ orbital magnetic moment) is clearly visible, illustrating the possible role played by the Pt electrons in the appearance of MCA.[34] From the XMCD spectra, we can determine directly the ratio m_{orb}/m_{spin}, which does not depend on the isotropic absorption cross section, the

TABLE I. The experimental (m_{orb}^{exper}) and theoretical (m_{orb}^{theor}) Co-$3d$ and Pt-$5d$ orbital magnetic moments as a function of the angle γ between the spin quantization axis and the normal to the surface. The calculated number of holes for Co and Pt are 2.628 and 2.480, respectively. Notice that while the theory underestimates the orbital magnetic moments, it reproduces nicely the trends as a function of γ. The magnetic moments are expressed in μ_B per atom. The error for the experimental values is of the order of 10%, larger than the experimental error bars, 4%, estimated in the case of Fe and Co (Ref. 24).

γ	$m_{orb}^{exper}(3d)$	$m_{orb}^{theor}(3d)$
0°	0.26	0.11
30°	0.24	0.09
45°	0.17	0.08
60°	0.11	0.05
γ	$m_{orb}^{exper}(5d)$	$m_{orb}^{theor}(5d)$
10°	0.09	0.06
60°	0.06	0.03

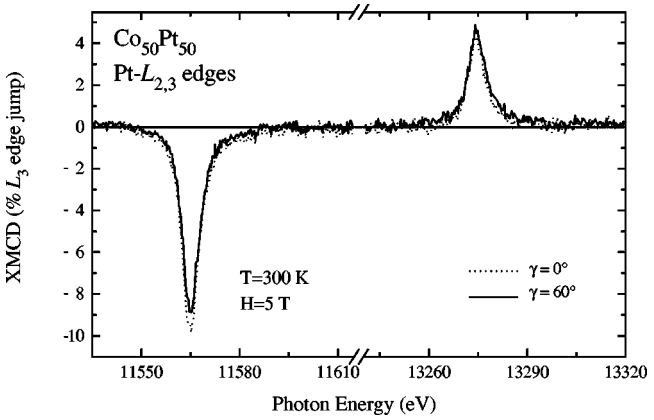

FIG. 8. XMCD signals (corrected for the finite rate of circular polarization) recorded at the $L_{2,3}$ of Pt in a $Co_{50}Pt_{50}$ thin film. The corresponding XAS spectra have been normalized by adjusting the step-height ratio to 2.2 (Ref. 34). $\gamma=10°$, dots; $\gamma=60°$, solid line.

number of holes and the degree of circular polarization [0.9 (Ref. 37)]. We found $m_{orb}/m_{spin}=0.27$ and 0.16 for $\gamma=10°$ and 60°, respectively. This illustrates the strong MCA since the spin magnetic moment is an isotropic quantity. The Pt-5d orbital and spin magnetic moments have been derived from the application of the sum rules, following a standard procedure: (i) the L_3 and L_2 XAS spectra are normalized in a ratio of 2.2 to account for a difference in the $\langle 5d|r|2p_{1/2}\rangle$ and $\langle 5d|r|2p_{3/2}\rangle$ radial matrix elements and (ii) the 5d isotropic absorption cross section per 5d hole is expressed in terms of the difference in the XAS spectra measured at the L_3 (L_2) edge of Pt in the $Co_{50}Pt_{50}$ thin film and at the L_3 (L_2) edge of Au in a $Cu_{50}Au_{50}$ foil.[34,38] Taking into account the number of nonmagnetic Pt atoms in the buffer layer, we found $m_{orb}/(h_{5d}^{Pt}-h_{5d}^{Au})=0.09\mu_B$ and $0.06\mu_B$ (per Pt atom) for $\gamma=10°$ and 60°, respectively.[39] Keeping in mind that the MCA is related to both the anisotropy of the orbital magnetic moment and the strength of the spin-orbit coupling, we emphasize that the role played by the 5d orbital magnetic moment, itself, is certainly non-negligible. Moreover, the anisotropy in the 5d orbital magnetic moment is larger than the one found in a $CoPt_3$ thin film grown at 690 K, in agreement with the larger anisotropy found from torque measurement.[34] Finally, in the determination of the m_{orb}/m_{spin} ratio, we have implicitly assumed that the contribution of the magnetic dipole term to the effective spin magnetic moment is negligible. This assumption is to some extent justified due to the finding of an isotropic effective spin magnetic moment, which should be attributed to the strong delocalization of the 5d electrons.[38] We found $m_{spin}^{eff}/(h_{5d}^{Pt}-h_{5d}^{Au})=0.35\,\mu_B$ and $0.36\,\mu_B$ (per Pt atom), for $\gamma=10°$ and 60°, respectively.

III. THEORETICAL STUDY

In this section we present our *ab initio* investigation of the XMCD and the magnetic properties of the $Co_{50}Pt_{50}$ system. A similar study has been already performed for the Fe nitrides.[9] We will first present our theoretical model used to calculate the XMCD spectra, the magnetic moments and the MCA. In a second part, the results of our calculations will be discussed and compared to experiment.

A. Theoretical model

The calculation of the x-ray absorption for left- and right-circularly polarized x-ray light is implemented within the local spin-density approximation (LSDA) by means of the all-electron fully relativistic and spin-polarized full-potential muffin-tin orbital method (LMTO).[40] The space within this method is divided in two regions: the nonoverlapping spheres (muffin-tin spheres) centered in each atom and the interstitial region. The muffin-tin potential is developed over the lattice harmonics of the system and the rest of the potential is treated using fast Fourier transform. The core electrons are spin polarized and their electronic states are obtained by solving iteratively the Dirac equation. For the valence electrons, the spin-orbit coupling is added to the semirelativistic Hamiltonian; and the total Hamiltonian is solved self-consistently. To calculate the polarization-dependent cross section we considered the spin quantization axis along the direction of the x-ray beam like in the XMCD experimental setup presented in Sec. II B. With respect to this axis, we define the left- and right-circular polarization, which corresponds to the photon helicity $(+\hbar)$ and $(-\hbar)$, respectively. We allowed only dipole electron-photon interactions: $\hat{\mathbf{e}}_{\pm}\cdot\mathbf{p}=1/\sqrt{2}(\nabla_x\pm\imath\nabla_y)$. The absorption cross sections $\mu_{\pm}$ for left- $(+)$ and right- $(-)$ circular polarized x-ray calculated at the relativistic $j_{\pm}$ $(l\pm\frac{1}{2})$ core level in the dipole approximation are given by

$$\mu_{\pm}(\omega)=\frac{2\pi}{\hbar}\sum_{m_{j_{\pm}}}\sum_{n,\mathbf{k}}|\langle j_{\pm}m_{\pm}|\hat{\mathbf{e}}_{\pm}\cdot\mathbf{p}|n\mathbf{k}\rangle|^2 \times\delta(\hbar\omega-E_{n,\mathbf{k}}+E_{j_{\pm}}), \quad (2)$$

where the first sum runs over the core initial states and the second one over the final unoccupied states.

In the above expression, we have neglected the rearrangement of the electronic cloud after the electron-photon excitation due to the creation of the core hole. This charge-relaxation process in the case of 3d ferromagnets should be comparable to the electron-hole recombination, so that the final states are at some extend affected. The local spin-density approximation is inadequate for the description of the physical process involving the electron-hole recombination.[41] More details about the inclusion of the core hole will be discussed in the XMCD subsection.

To compute the electronic properties of $Co_{50}Pt_{50}$ we used the experimental lattice constants and a unit cell containing one atom of Co and one of Pt (see Fig. 1). We allowed the spin-polarized core electrons to relax during the self-consistent calculation, and we used the parametrization of von Barth and Hedin for the exchange-correlation potential and energy. [44] We shifted our $\mathbf{k}$ mesh rigidly by half a step along the x, y, and z axis from the Γ point in the Brillouin zone (BZ), to avoid high symmetry directions and planes in the BZ and consequently any degenerate eigenvalues.

The magnetic anisotropy energy (MAE) can be computed directly using *ab initio* methods; it is defined as the difference between the total energy for two different spin quantization axis. The biggest contribution to MAE comes usually from the MCA, whose origin is the spin-orbit coupling, but there are also contributions related to the strains induced when we apply a field and oblige the magnetization to rotate

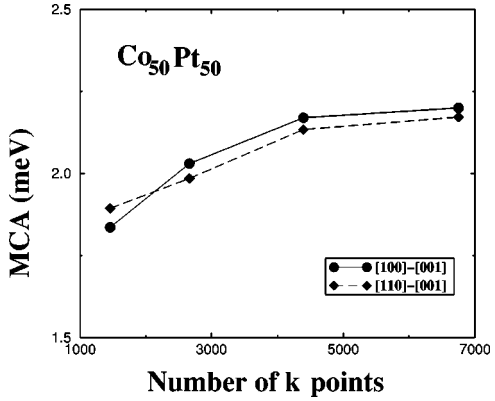

FIG. 9. Difference in the total energy between one of the two hard in-plane axis, [110] or [100], and the easy [001] axis [i.e., magnetocrystalline anisotropy (MCA) energy] as a function of the number of **k** points in the Brillouin zone. The small difference observed in the MCA for the two different in-plane axis is correlated to the symmetry of the crystal structure.

from its easy axis. The last contribution, known also as magnetoelastic energy, is not taken into account in our calculations, so from now on we will refer ourselves only to MCA. The number of **k** points that we use in the BZ to perform the integrations depends strongly on the interplay between the contributions to MCA from the Fermi surface and the band contribution to the total energy. [45] When the former contribution to the MCA is important, a large number of **k** points is needed to describe accurately the Fermi surface.

B. Theoretical results and discussion

1. MCA

Figure 9 shows the results of the calculations of the MCA and its convergence with the number of **k** points used to perform the **k**-point integral over the Brillouin zone. The MCA for our system is the difference in total energy between one of the two in-plane hard axis, [100] or [110], and the easy [001] axis. We see almost no difference between the MCA for the [100] and [110] axis and they both converge to about the same value of 2.2 meV, with respect to the number of **k** points. This finding confirms and supports the assumption of an in-plane isotropy of the spin and orbital magnetic moments. The calculated value can be compared with the experimental result of MCA of Eurin and Pauleve[5] of 1.3 meV/(unit cell), and our experimental value of 1.0 meV/(unit cell). Our computed value agrees also with the value of 1.5 meV/(unit cell), obtained by Sakuma using LMTO method in the atomic-sphere approximation.[46]

2. Magnetic moments

The theoretical spin magnetic moments are calculated directly by integrating the partial density of states inside each muffin-tin sphere. The small contribution of the interstitial region to the total spin magnetic moment (one order of magnitude smaller than the spin moment on the Pt atom), which is difficult to attribute to a specific atom, is neglected. We have also calculated the orbital magnetic moments induced by the spin-orbit coupling. The number of holes in the *d* bands of Co and Pt, required by the optical sum rules to extract the spin and orbital magnetic moments from the experimental XMCD spectra, are obtained by projecting each muffin-tin sphere spin density of states on the *d*-channel angular momentum. The values we used are 2.628 for Co and 2.480 for Pt. In Tables I and II, we present the experimental and theoretical orbital and spin magnetic moments, obtained for different orientations of the spin quantization axis. The Pt spin magnetic moment is purely induced by hybridization and spin-orbit coupling. We expect a reasonable agreement for the spin magnetic moment, where any difference should come from the fact that the sum rules are derived from an atomic theory and their application to itinerant electrons, although useful, is not exact, especially for Pt where the 5*d* states are much more delocalized than the 3*d* states of Co.[26] At the precision of the experimental results, there is indeed a good agreement between the experimental and theoretical spin magnetic moments. In contrast, there is a strong discrepancy for the orbital magnetic moment since LSDA significantly underestimates the orbital moment.[47] However, the behavior of the orbital magnetic moment as a function of the incident angle γ is the same for both experimental and theoretical results. For instance, the computed 3*d* orbital magnetic moment for $\gamma=60°$ is 0.45 times the value for $\gamma=0°$, while the experimental ratio is 0.42. This shows that even if LSDA underestimates the orbital moments, it describes correctly the trends, with respect to the angle γ.

TABLE II. The experimental (m_{spin}^{exper}) and theoretical (m_{spin}^{theor}) Co-3*d* and Pt-5*d* spin magnetic moments. The Pt spin magnetic moment is purely induced by hybridization and spin-orbit coupling. The magnetic moments are expressed in μ_B per atom. The error for the experimental values varies from 6% up to 10%, and it is larger than the experimental error bars, 4%, estimated in the case of Fe and Co (Ref. 24).

	m_{spin}^{exper}	m_{spin}^{theor}
Co	1.76	1.79
Pt	0.35	0.37

3. XMCD

As mentioned in Sec. III A we expect a better agreement between theory and experiment for Pt than for Co, concerning the XMCD spectra. In Fig. 10 we have plotted the absorption and the XMCD spectra of Co for $\gamma=0°$. We have scaled our spectra in a way that the experimental and theoretical L_3 peaks in the absorption spectra have the same intensity. The energy difference between the L_3 and L_2 peaks is given by the spin-orbit splitting of the $p_{1/2}$ and $p_{3/2}$ core states of 14.8 eV, and is in good agreement with experiment. But the intensity of the L_2 peak is larger than the corresponding experimental peak. We convoluted our theoretical spectra using a Lorentzian width of 0.9 eV and a Gaussian width of 0.4 eV as proposed by Ebert.[8] The Gaussian represents the experimental resolution while the Lorentzian corresponds to the width of the core hole. As mentioned above, this broadening effect is important for 3*d* transition metals like Co. The high intensity of the calculated L_2 edge makes the theoretical XMCD integrated L_3/L_2 branching ratio of 1.32 much smaller than the experimental ratio of 1.72. This dis-

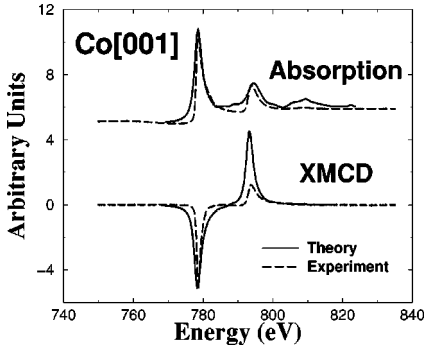

FIG. 10. Experimental and theoretical isotropic-XAS (XMCD) spectra at the Co $L_{2,3}$ edges ($\gamma=0°$). The theoretical spectra have been broadened by a combination of a Lorentzian and a Gaussian function to account for core-hole effects and experimental resolution, respectively. We observe a semiquantitative agreement with experiment, although the so-called branching ratio is underestimated by our calculations.

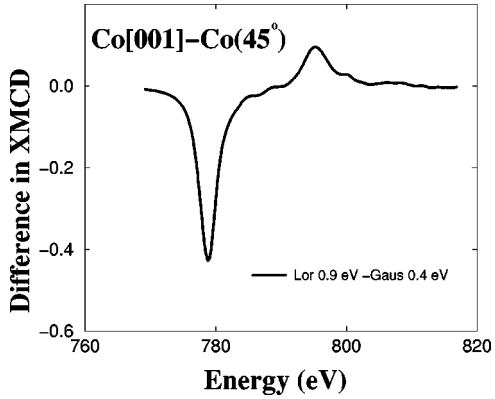

FIG. 11. Difference in the XMCD signal at the Co $L_{2,3}$ edges obtained for two different orientation of the spin quantization axis with respect to the [001] direction (Ref. 48).

crepancy of the L_3/L_2 branching ratio is not surprising since we do not take into account the photoelectron core-hole interaction.

An attempt to include the core hole interaction on the calculated XAS was made by one of us[41] using the final-state rule, i.e., assuming that the final-state energies are measured and the dynamics of the excitation process are neglected. This results in a static description of the core hole. The atom with a core hole is embedded in a crystal using a supercell geometry. It was found that the screening of the core hole is such that the atom with the core hole acquired the same number of valence electrons as the next atom in the periodic table, i.e., an Fe atom with a core hole developed a spin magnetic moment closer to that of bulk Co, and the Co excited atom magnetic moment is closer to that of bulk Ni, and the Ni excited atom has no magnetic moment like bulk copper (see Ref. 41 for details). This simple static picture of the electron-hole interaction is insufficient for the description of XMCD because the XMCD through the use of sum rules describes the ground-state magnetic properties. Brouder *et al.*[12] used also the final-state rule to account for the core hole effect on the *K* edge of Fe. Here the core hole is located in the 1*s* state and the final state is of *p* character. Both the XAS and XMCD at the *K* edge were not much affected by the presence of the core hole because the Fe *p* states did not participate much to the screening of the core hole. A comparison with experiment did not show much of an improvement. On the other hand, the calculation of Ankudinov *et al.*,[15] using multiple scattering cluster code, of the *K*-edge XAS of paramagnetic BN showed that the final-state rule works better than in the case of the $L_{2,3}$ edge of 3*d* ferromagnets. However, it is surprising that the relative change of the peak intensities in the *K*-edge spectrum is much more pronounced than that of the *p* density of states despite that the dipole matrix elements are known to have a weak energy dependence. Finally, Schwitalla and Ebert performed relativistic calculations using time-dependent density functional theory to account for the core-hole effect but their results for the $L_{2,3}$ branching ratio of the late transition metals (Fe, Ni, and Co) were in worse agreement with experiment than those without core-hole effect.[42] To take effectively the core-hole photoexcited electron interaction, including the dynamics of the relaxation is a difficult task, and would require the calculation of a time-dependent two-particle Green's function.[43] In conclusion, we believe that a good description of the electron hole interaction should improve the branching ratio, and progress along the work of Zaanen *et al.*[43] is desirable.

Figure 11 shows the difference between the theoretical Co XMCD for two different directions of the spin quantization axis. We see clearly that there is a change in the XMCD signal, which is related to the change in the orbital magnetic moment between these two directions and consequently this XMCD anisotropy should be proportional to the underlying MCA.

In contrast to what is obtained for Co, the results for the Pt atoms (Fig. 12) show a better agreement with experiment, due to the fact that the core hole effect is less intense (core hole much deeper compared to Co). For the Pt atom we used both a Lorentzian (1 eV) and a Gaussian (1 eV) to represent the core hole effect and a Gaussian of 1 eV width for the experimental resolution. The experimental and theoretical L_2 and L_3 edges are separated by a spin-orbit splitting of the $2p$

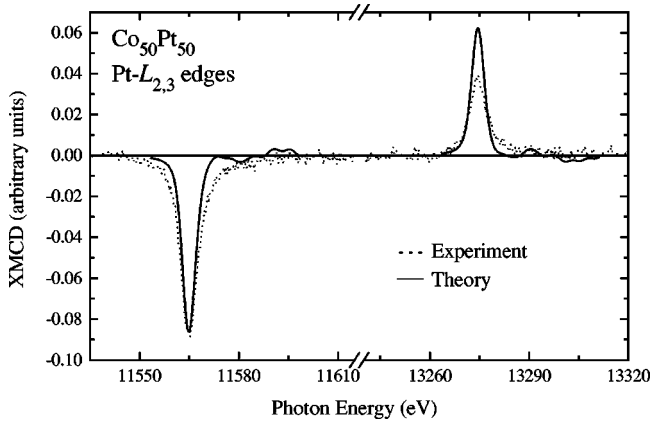

FIG. 12. Experimental and theoretical XMCD signals at the Pt $L_{2,3}$ edges ($\gamma=10°$). The theoretical spectra have been broadened by a combination of a Lorentzian and a Gaussian function to account for core-hole effects and experimental resolution, respectively. We observe a semiquantitative agreement with experiment, although the so-called branching ratio is underestimated by our calculations.

core states of 1709 and 1727 eV, respectively. The width of both L_2 and L_3 edges is comparable to experiment, but the calculated L_2 edge is much larger. This produces a calculated integrated branching ratio of 1.49 which is much smaller than the experimental ratio of 2.66. Here again the theory underestimates the branching ratio.

IV. CONCLUSION

We have investigated the magnetic properties of the ordered $Co_{50}Pt_{50}$ alloy from both an experimental and a theoretical point of view. From angle-dependent x-ray magnetic circular dichroism measurements, we have investigated the anisotropic $3d$-$5d$ hybridization and the strong Pt spin-orbit coupling that favor a large perpendicular magnetocrystalline anisotropy. The derived spin magnetic moments were found to be in good agreement with the results of our *ab initio* calculations. We showed that our theory is capable of reproducing the experimental trends of the variation of the orbital magnetic moment as the function of the direction of the spin quantization axis. The calculation of the x-ray magnetic circular dichroic signal ignoring the electron-hole recombination effect provides a semiquantitative agreement with the experimental spectra of both Co and Pt edges. The underestimation of the $L_{2,3}$ branching ratio remains a great challenge for theorists and further theoretical development along the line proposed by Schwitalla and Ebert[42] is needed to bring the theory at the level of the experiment.

ACKNOWLEDGMENTS

We are grateful to J.M. Wills for providing us with his FP-LMTO code. W.G. thanks C. Uhlaq-Bouillet for her precious help in the transmission electron microscopy measurements. Finally, we would like to thank the staff of the ID12A and ID12B beamlines at ESRF for the excellent operation conditions and their advice during the experiments. The calculations were performed using the facilities of the Institut de Développement et des Ressources en Informatique Scientifique (IDRIS) under Project No. 981074.

*Permanent address: Institut de Physique et Chimie des Matériaux de Strasbourg (IPCMS), 23 rue du Loess, 67037 Strasbourg Cedex, France.

[1] P. W. Rooney, A. L. Shapiro, M. Q. Tran, and F. Hellman, Phys. Rev. Lett. **75**, 1843 (1995).

[2] M. Maret, M. C. Cadeville, R. Poinsot, A. Herr, E. Baurepaire, and C. Monier, J. Magn. Magn. Mater. **166**, 45 (1997).

[3] C. Meneghini, M. Maret, M. C. Cadeville, and J. L. Hazemann, J. Phys. IV Colloq. **7**, C2-1115 (1997).

[4] E. Beaurepaire, M. Maret, V. Halté, J.-C. Merle, A. Daunois, and J.-Y. Bigot, Phys. Rev. B **58**, 12 134 (1998).

[5] P. Eurin and J. Pauleve, IEEE Trans. Magn. **5**, 216 (1969).

[6] D. Weller, J. Stöhr, R. Nakajima, A. Carl, M. G. Samant, C. Chappert, R. Mégy, P. Beauvillain, P. Veillet, and G. A. Held, Phys. Rev. Lett. **75**, 3752 (1995).

[7] J. Stöhr, J. Electron Spectrosc. Relat. Phenom. **75**, 253 (1995).

[8] H. Ebert, Rep. Prog. Phys. **59**, 1665 (1996).

[9] M. Alouani, J. M. Wills, and J. W. Wilkins, Phys. Rev. B **57**, 9502 (1998).

[10] G. Schütz, M. Knülle, R. Wienke, W. Wilhelm, W. Wagner, P. Kienle, R. Zeller, and R. Frahm, Z. Phys. B: Condens. Matter **75**, 495 (1989).

[11] C. Brouder and M. Hikam, Phys. Rev. B **43**, 3809 (1991).

[12] C. Brouder, M. Alouani, and K. H. Bennemann, Phys. Rev. B **54**, 7334 (1996).

[13] G. Y. Guo, Phys. Rev. B **57**, 10 295 (1998).

[14] A. L. Ankudinov and J. J. Rehr, Phys. Rev. B **56**, 1712 (1997).

[15] A. L. Ankudinov, B. Ravel, J. J. Rehr, and S. Conradson, Phys. Rev. B **58**, 7565 (1998).

[16] G. van der Laan and B. T. Thole, Phys. Rev. B **43**, 13 401 (1991).

[17] J. -L. Vassent, Ph.D. thesis, CEA-DRFMC-Grenoble, 1995.

[18] G. R. Harp, D. Weller, T. A. Rabedeau, R. F. C. Farrow, and R. F. Marks, in ''*Magnetic Ultrathin Films–Multilayers and Surfaces*,'' Interfaces, and Characterization, edited by B. T. Jonker *et al.*, MRS Synposia Proceedings No. 313 (Materials Research Society, Pittsburgh, 1993), p. 493.

[19] V. Gehanno, A. Marty, B. Gilles, and Y. Samson, Phys. Rev. B **55**, 12 552 (1997).

[20] This effect is purely elastic (i.e., results from the large difference in the size of the Pt and Co atoms) since the free surface energy is almost similar for Co and Pt.

[21] H. Miyajima and K. Sato, J. Appl. Phys. **47**, 4669 (1976).

[22] B. T. Thole, P. Carra, F. Sette, and G. van der Laan, Phys. Rev. Lett. **68**, 1943 (1992).

[23] P. Carra, B. T. Thole, M. Altarelli, and X. Wang, Phys. Rev. Lett. **70**, 694 (1993).

[24] C. T. Chen, Y. U. Idzerda, H.-J. Lin, N. V. Smith, G. Meigs, E. Chaban, G. H. Ho, E. Pellegrin, and F. Sette, Phys. Rev. Lett. **75**, 152 (1995).

[25] The magnetic dipole term can represent a significant contribution to the effective spin magnetic moment [up to 50% at the (001) surface of Ni] (Ref. 26).

[26] R. Wu and A. J. Freeman, Phys. Rev. Lett. **73**, 1994 (1994).

[27] From the beginning of 1960s, numerous theoretical and experimental studies have outlined the possible connection between the anisotropy of the magnetization and the magnetocrystalline anisotropy energy [see P. Escudier, Ann. Phys. (N.Y.) **9**, 125 (1975) for an exhaustive bibliography]. However, the first relation between MCA and the different relevant physical parameters that govern MCA (namely, the spin-orbit coupling, the orbital magnetic moment, and the crystal field) was derived by Bruno in 1989 (Ref. 28).

[28] P. Bruno, Phys. Rev. B **39**, 865 (1989).

[29] A critical discussion of Bruno's relation (Ref. 28) can be found in the following references: P. Bruno, in *Ferienkurse des Forschungszentrum* (Jülich, Jülich, 1993), Vol. 24, p. 24; B. Újfalussy, L. Szunyogh, P. Bruno, and P. Weinberger, Phys. Rev. Lett. **77**, 1805 (1996); O. Hjortstam, K. Baberschke, J. M. Wills, B. Johansson, and O. Eriksson, Phys. Rev. B **55**, 15 026 (1997); A. N. Anisimov, M. Farle, P. Poulopoulos, W. Platow, K. Baberschke, P. Isberg, R. Wäppling, A. M. N. Niklasson, and O. Eriksson, Phys. Rev. Lett. **82**, 2390 (1999).

[30] D. S. Wang, R. Wu, and A. J. Freeman, Phys. Rev. B **47**, 14 932 (1989).

[31] G. van der Laan, J. Phys.: Condens. Matter **10**, 3239 (1998).

[32] J. Goulon, N. B. Brookes, C. Gauthier, J. B. Goedkoop, C. Goulon-Ginet, M. Hagelstein, and A. Rogalev, Physica B **208&209**, 199 (1995).

[33] N. Drescher, G. Snell, U. Kleineberg, H.-J. Stock, N. Müller, U. Heinzmann, and N. B. Brookes, Rev. Sci. Instrum. **68**, 1939 (1997).

[34] W. Grange, M. Maret, J.-P Kappler, J. Vogel, A. Fontaine, F. Petroff, G. Krill, A. Rogalev, J. Goulon, M. Finazzi, and N. B. Brookes, Phys. Rev. B **58**, 6298 (1998).

[35] G. van der Laan, Phys. Rev. B **57**, 5250 (1998).

[36] One should keep in mind that the real situation is more complicated since, in principle, we cannot treat separately the contribution of the Co and Pt electrons to the MCA. It is, however, clear that the appearance of a chemical long-range order will increase the value of the MCA [L. Néel, J. Phys. Radium **4**, 15 (1954)].

[37] L. Varga, C. Giles, C. Neumann, A. Rogalev, C. Malgrange, J. Goulon, and F. de Bergevin, J. Phys. IV **7**, C2-309 (1997).

[38] J. Vogel, A. Fontaine, V. Cross, F. Petroff, J.-P. Kappler, G. Krill, A. Rogalev, and J. Goulon, Phys. Rev. B **55**, 3663 (1997).

[39] The quantity $(h_{5d}^{Pt}-h_{5d}^{Au})$ flows from the procedure that we use to get an accurate determination of the isotropic absorption cross section. It denotes the difference in $5d$ hole count between Pt in the $Co_{50}Pt_{50}$ thin film and Au in a $Cu_{50}Au_{50}$ reference foil. This value is computed by our theory and is equal to 1.09.

[40] J. M. Wills and B. R. Cooper, Phys. Rev. B **36**, 3809 (1987); M. Alouani and J. M. Wills, *ibid.* **54**, 2480 (1996); J. Wills, O. Eriksson, M. Alouani, and D. L. Price, *Electronic Structure and Physical Properties of Solids: The Uses of the LMTO Method*, edited by Hugues Dreyssé, Lecture Notes in Phyiscs (Springer, New York, 2000), p. 535.

[41] M. Alouani, Phys. Rev. B **49**, 16 038 (1994).

[42] J. Schwitalla and H. Ebert, Phys. Rev. Lett. **80**, 4586 (1998).

[43] J. Zaanen, G. A. Sawatzky, J. Fink, W. Speier, and J. C. Fuggle, Phys. Rev. B **32**, 4905 (1985).

[44] U. von Barth and L. Hedin, J. Phys. C **5**, 1629 (1972).

[45] I. V. Solovyev, P. H. Dederichs, and I. Mertig, Phys. Rev. B **52**, 13 419 (1995).

[46] A. Sakuma. J. Phys. Soc. Jpn. **63**, 3053 (1994); The LMTO-ASA method used in this paper takes into account only the spherical part of the potential, ignores the interstitial region and treats the spin-orbit coupling in the manner given by Andersen (Ref. 40). Using the force theorem [A.R. Macintosh and O.K. Andersen, *Electrons at the Fermi Surface*, edited by M. Springfold (Cambridge University Press, Cambridge, 1980)], Sakuma calculated the MCA as a difference between sums of eigenvalues of the Kohn-Sham equations over the occupied states

$$\Delta E=\sum_{i,\mathbf{k}}^{occ} \epsilon_i([100],\mathbf{k})-\sum_{i,\mathbf{k}}^{occ} \epsilon_i([001],\mathbf{k})$$

This way of calculating the MCA does not take explicitly into account the exchange-correlation contributions.

[47] Brooks has used a term derived from the atomic theory, $-I\hat{L}\hat{L}_z$ but its use in the case of itinerant electrons is not always sufficient to describe electronic orbital moment [M. S. S. Brooks, Physica B **130**, 6 (1985)]. A more sophisticated approach called current and spin-density functional theory (CSDFT) has been developed by Vignale and Rasolt, which treats in the same footing the Kohn-Sham and the Maxwell equations [see, G. Vignale and M. Rasolt, Phys. Rev. B **37**, 10 685 (1988)]. This formalism is complicated and hence computationally difficult to include in *ab initio* methods.

[48] This behavior could be difficult to extract from an experiment since a slight change in the energy for two measurements could lead to a big change in the difference in XMCD anisotropy.